HNPS Advances in Nuclear Physics

Vol 15 (2006)

HNPS2006

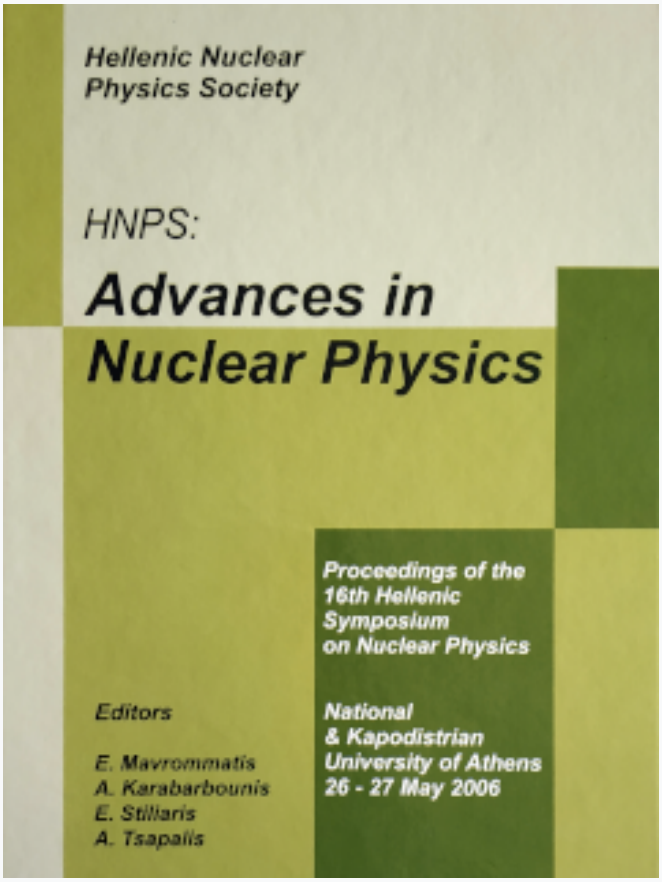

Connecting the X(5)-β2, X(5)-β4, and X(3) models to the shape/phase transition region of the Interacting Boson Model

E. A. McCutchan, D. Bonatsos, R. F. Casten

doi: 10.12681/hnps.2628

Connecting the X(5)-β^2, X(5)-β^4, and X(3) models to the shape/phase transition region of the Interacting Boson Model

E. A. McCutchan[a], Dennis Bonatsos[b] and N. V. Zamfir[c]

[a]Wright Nuclear Structure Laboratory, Yale University, New Haven, Connecticut 06520-8124, USA

[b]Institute of Nuclear Physics, National Centre for Scientific Research "Demokritos", GR-15310 Aghia Paraskevi, Attiki, Greece

[c]National Institute of Physics and Nuclear Engineering, Bucharest-Magurele, Romania

The parameter independent (up to overall scale factors) predictions of the X(5)-β^2, X(5)-β^4, and X(3) models, which are variants of the X(5) critical point symmetry developed within the framework of the geometric collective model, are compared to two-parameter calculations in the framework of the interacting boson approximation (IBA) model. The results show that these geometric models coincide with IBA parameters consistent with the phase/shape transition region of the IBA for boson numbers of physical interest (close to 10). ^{186}Pt and ^{172}Os are identified as good examples of X(3), while ^{146}Ce, ^{174}Os and ^{158}Er, ^{176}Os are identified as good examples of X(5)-β^2 and X(5)-β^4 behavior respectively.

1. INTRODUCTION

Critical point symmetries [1,2], describing nuclei at points of shape/phase transitions between different limiting symmetries, have recently attracted considerable attention, since they lead to parameter independent (up to overall scale factors) predictions which are found to be in good agreement with experiment [3–6]. The X(5) critical point symmetry [2], was developed to describe analytically the structure of nuclei at the critical point of the transition from vibrational [U(5)] to prolate axially symmetric [SU(3)] shapes. The solution involves a five-dimensional infinite square well potential in the β collective variable and a harmonic oscillator potential in the γ variable. The success of the X(5) model in describing the properties of some nuclei with parameter free (except for scale) predictions has led to considerable interest in such simple models to describe transitional nuclei. Since its development, numerous extensions involving either no free parameters or a single free parameter have been developed. Those approaches which involve a single parameter include replacing the infinite square well potential with a sloped well potential [7], exact decoupling of the β and γ degrees of freedom [8], and displacement of the infinite square well potential, or the confined β-soft model [9]. Parameter free variants of the X(5) model include the X(5)-β^2 and X(5)-β^4 models [10], in which the infinite square well potential is replaced by a β^2 and a β^4 potential respectively, as well as the X(3) model [11], in which

the γ degree of freedom is frozen to $\gamma = 0$, resulting in a three-dimensional Hamiltonian, in which an infinite square well potential in β is used.

Prior to these simple geometric models, shape/phase transitions were investigated [12] within the interacting boson approximation (IBA) model [13] by constructing the classical limit of the model, using the coherent state formalism [14,15]. Using this method it was shown [12,15] that the shape/phase transition between the U(5) and SU(3) limiting symmetries is of first order, while the transition between the U(5) and O(6) (γ-unstable) limiting symmetries is of second order. Furthermore, the region of phase coexistence within the symmetry triangle [16] of the IBA has been studied [17–19] and its borders have been determined [20,21], while a similar structural triangle for the geometric collective model has been constructed [22].

It is certainly of interest to examine the extent to which the parameter free (up to overall scale factors) predictions of the various critical point symmetries and related models, built within the geometric collective model, are related to the shape/phase transition region of the IBA. It has already been found [23] that the X(5) predictions cannot be exactly reproduced by any point in the two-parameter space of the IBA, while best agreement is obtained for parameters corresponding to a point close to, but outside the shape/phase transition region of the IBA. In the present work we examine the extent to which the predictions of the X(5)-β^2, X(5)-β^4, and X(3) models can be reproduced by two-parameter IBA calculations using boson numbers of physical interest (close to 10) and the relation of these geometrical models to the shape/phase transition region of the IBA. Even-even nuclei corresponding to reasonable experimental examples of the manifestation of the X(3), X(5)-β^2, and X(5)-β^4 models are also identified.

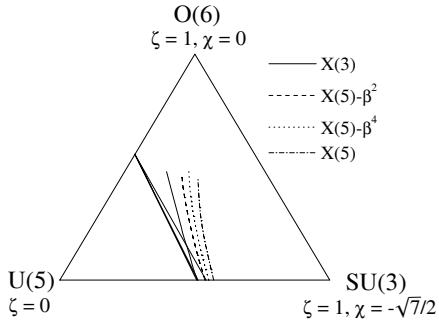

Figure 1. IBA symmetry triangle illustrating the dynamical symmetry limits and their corresponding parameters. The phase transition region of the IBA, bordered by ζ^* on the left and by ζ^{**} on the right, as well as the loci of parameters which reproduce the $R_{4/2}$ ratios of X(3) (2.44), X(5)-β^2 (2.65), X(5)-β^4 (2.77), and X(5) (2.90) are shown for $N_B = 10$. The line defined by $\zeta_{\rm crit}$ is also shown, lying to the right of the left border and almost coinciding with it.

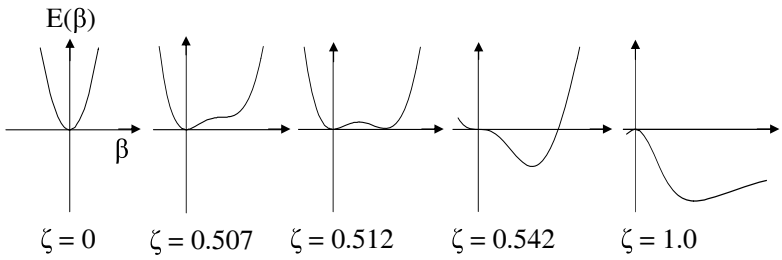

Figure 2. Evolution with ζ of IBA total energy curves for $N_B = 10$ and $\chi = -1.32$.

2. THE IBA HAMILTONIAN AND SYMMETRY TRIANGLE

The study of shape/phase transitions in the IBA is facilitated by writing the IBA Hamiltonian in the form [18,20]

$$H(\zeta,\chi) = c\left[(1-\zeta)\hat{n}_d - \frac{\zeta}{4N_B}\hat{Q}^\chi\cdot\hat{Q}^\chi\right], \tag{1}$$

where $\hat{n}_d = d^\dagger\cdot\tilde{d}$, $\hat{Q}^\chi = (s^\dagger\tilde{d} + d^\dagger s) + \chi(d^\dagger\tilde{d})^{(2)}$, N_B is the number of valence bosons, and c is a scaling factor. The above Hamiltonian contains two parameters, ζ and χ, with the parameter ζ ranging from 0 to 1, and the parameter χ ranging from 0 to $-\sqrt{7}/2 = -1.32$. With this parameterization, the entire symmetry triangle of the IBA, shown in Fig. 1, can be described, along with each of the three dynamical symmetry limits of the IBA. The parameters (ζ,χ) can be plotted in the symmetry triangle by converting them into polar coordinates [24]

$$\rho = \frac{\sqrt{3}\zeta}{\sqrt{3}\cos\theta_\chi - \sin\theta_\chi}, \qquad \theta = \frac{\pi}{3} + \theta_\chi, \tag{2}$$

where $\theta_\chi = (2/\sqrt{7})\chi(\pi/3)$.

Using the coherent state formalism of the IBA [13–15] one can obtain the scaled total energy, $E(\beta,\gamma)/(cN_B)$, in the form [19]

$$\mathcal{E}(\beta,\gamma) = \frac{\beta^2}{1+\beta^2}\left[(1-\zeta) - (\chi^2+1)\frac{\zeta}{4N_B}\right] - \frac{5\zeta}{4N_B(1+\beta^2)}$$

$$-\frac{\zeta(N_B-1)}{4N_B(1+\beta^2)^2}\left[4\beta^2 - 4\sqrt{\frac{2}{7}}\chi\beta^3\cos 3\gamma + \frac{2}{7}\chi^2\beta^4\right], \tag{3}$$

where β and γ are the two classical coordinates, related [13] to the Bohr geometrical variables [25].

As a function of ζ, a shape/phase coexistence region [17] begins when a deformed minimum, determined from the condition $\frac{\partial^2\mathcal{E}}{\partial\beta^2}|_{\beta_0\neq 0} = 0$, appears in addition to the spherical minimum, and ends when only the deformed minimum remains. The latter is achieved

when $\mathcal{E}(\beta,\gamma)$ becomes flat at $\beta = 0$, fulfilling the condition [20] $\frac{\partial^2 \mathcal{E}}{\partial \beta^2}|_{\beta=0} = 0$, which is satisfied for

$$\zeta^{**} = \frac{4N_B}{8N_B + \chi^2 - 8}. \tag{4}$$

The former, ζ^*, can be derived from the results of Ref. [26]. For $\chi = -\sqrt{7}/2$ this point is given by

$$\zeta^* = \frac{(896\sqrt{2} + 656R)N_B}{-1144\sqrt{2} + 123R + (1536\sqrt{2} + 164R)N_B} \tag{5}$$

where

$$R = \sqrt{\frac{35456}{15129} + \frac{32\ 6^{2/3}}{41}} - \sqrt{\frac{70912}{15129} - \frac{32\ 6^{2/3}}{41} + \frac{3602816}{15129\sqrt{1108 + 369\ 6^{2/3}}}} \tag{6}$$

In between there is a point, $\zeta_{\rm crit}$, where the two minima are equal and the first derivative of $\mathcal{E}_{min}$, $\partial \mathcal{E}_{min}/\partial\zeta$, is discontinuous, indicating a first-order phase transition. For $\chi = -\sqrt{7}/2$ this point is [21]

$$\zeta_{\rm crit} = \frac{16N_B}{34N_B - 27}. \tag{7}$$

Expressions for ζ^* and ζ_{crit} involving the parameter χ can also be deduced using the results of Ref. [26].

The range of ζ corresponding to the region of shape/phase coexistence shrinks with decreasing $|\chi|$ and converges to a single point for $\chi = 0$, which is the point of a second-order phase transition between U(5) and O(6), located on the U(5)–O(6) leg of the symmetry triangle (which is characterized by $\chi = 0$) at $\zeta = N_B/(2N_B - 2)$, as seen from Eq. (4). The phase transition region of the IBA is included in Fig. 1. For $N_B = 10$, it is clear that the left border of the phase transition region, defined by ζ^*, and the line defined by $\zeta_{\rm crit}$ nearly coincide. For $\chi = -1.32$, in particular, one has $\zeta^* = 0.507$ and $\zeta_{\rm crit} = 0.511$. Therefore in what follows we shall use $\zeta_{\rm crit}$ as the approximate left border of the phase transition region.

3. COMPARISON OF X(3), X(5)-β^2, AND X(5)-β^4 PREDICTIONS TO IBA

A basic structural signature is the yrast band energy ratio $R_{4/2} \equiv E(4_1^+)/E(2_1^+)$. A constant value of the $R_{4/2}$ ratio can be obtained in the IBA for a small range of ζ values (since both provide a measure of the quadrupole deformation) and a wider range of χ values. Figure 1 gives the loci of the parameters which reproduce the $R_{4/2}$ ratios of X(3) (2.44), X(5)-β^2 (2.65), X(5)-β^4 (2.77), and X(5) (2.90), for $N_B = 10$. As expected from the varying $R_{4/2}$ ratios, there is a smooth evolution of the lines from X(3) up through X(5), corresponding to an increase in the average ζ value. Relating to the phase/shape transition region of the IBA, the X(3) locus begins on the U(5)-SU(3) leg of the triangle close to the left border of the phase/shape transition region and then crosses it as the absolute value of χ decreases. The X(5)-β^2 locus starts within the right border of the phase/shape transition region on the bottom leg of the triangle, then diverges slightly

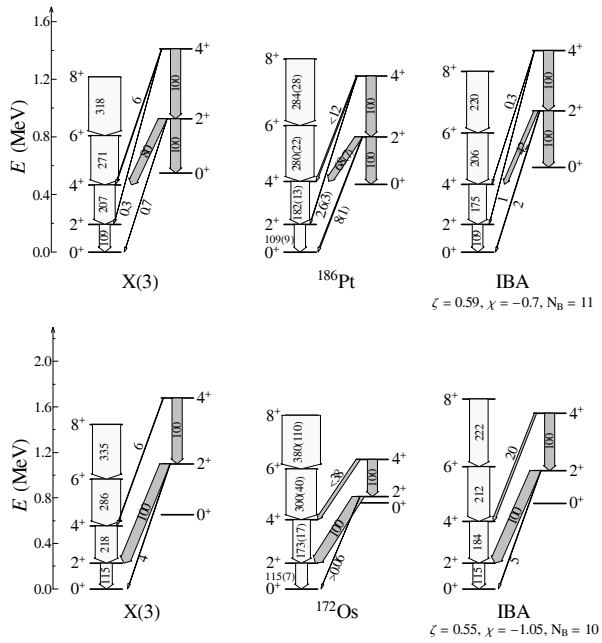

Figure 3. Comparison of the experimental data (middle) to the X(3) predictions (left) and IBA calculations (right) for ^{186}Pt (top) and ^{172}Os (bottom). The thicknesses of the arrows indicate the relative (gray arrows) and absolute (white arrows) $B(E2)$ strengths which are also labelled by their values. The absolute $B(E2)$ strengths are normalized to the experimental $B(E2; 2_1^+ \rightarrow 0_1^+)$ value in each nucleus. Experimental data taken from Refs. [32–34].

away from it. The X(5)-β^4 and X(5) loci lie just beyond the phase/shape transition region on the U(5)-SU(3) leg of the triangle, then move away from it. This evolution can be understood by considering the potentials used in these solutions. X(5)-β^2 uses a harmonic oscillator potential while X(5)-β^4 involves a potential intermediate between the β^2 potential and the infinite square well potential of X(5). Note that each of these modified versions of the X(5) solution are at some point closer to the phase/shape transition region of the IBA than X(5) itself.

Other observables (energy ratios, $B(E2)$ ratios) also lead to the conclusion that for boson numbers of physical interest (close to 10) the X(3) predictions are close to IBA predictions for parameter values close to the left border of the transition region of the IBA, while the X(5)-β^2 predictions are close to IBA predictions for parameter values close to the right border of the transition region of the IBA. One can see that fixing the parameter χ to -1.32 (i.e. insisting to stay along the bottom of the IBA symmetry triangle) and using $N_B = 10$ (a reasonable value for several rare earth nuclei), the level schemes of X(3), X(5)-β^2, and X(5)-β^4 can be well reproduced for the ζ values of $\zeta_{\rm crit} = 0.51$, $\zeta^{**} = 0.54$,

and 0.55 respectively. Treating χ as a free parameter improves the "IBA best fits" of these models only slightly, resulting (for $N_B = 10$) to (ζ, χ) parameter values of $(0.55, -0.92)$, $(0.57, -0.99)$, $(0.59, -1.03)$ for X(3), X(5)-β^2, and X(5)-β^4 respectively.

Since we have found that the X(3), X(5)-β^2, and X(5)-β^4 predictions are best reproduced by IBA Hamiltonians with $\chi = -1.32$, or close to it, it is instructive to study [21] the evolution with increasing ζ of the IBA total energy curves for $N_B = 10$ and $\chi = -1.32$, shown in Fig. 2. It is clear that at $\zeta = \zeta_{\rm crit}$, where the two minima are equal, the total energy curve can be quite well approximated by an infinite square well, which is the potential used in X(3), best reproduced with $\zeta = \zeta_{\rm crit}$. In contrast, at $\zeta = \zeta^{**}$ a deeper minimum at positive β starts to develop. The total energy curves at and beyond ζ^{**} are quite similar to the β^2 and β^4 potentials, when the latter are supplemented by a $L(L+1)/(3\beta^2)$ centrifugal term [8], found recently through the use of novel techniques allowing for the exact numerical diagonalization of the Bohr Hamiltonian [27–29].

4. COMPARISON OF X(3), X(5)-β^2, AND X(5)-β^4 PREDICTIONS TO EXPERIMENT

Several nuclei in the rare-earth region with $N = 90$ have been identified [5,6] as candidates for the X(5) critical point model. Therefore one obvious region to look for candidates for the X(3), X(5)-β^2, and X(5)-β^4 models is in the neighbors to these nuclei. In addition, within the framework of the IBA, detailed fits [30,31] to Os and Pt isotopes have identified nuclei which lie close to the shape/phase transition region of the IBA. Candidates can be identified by considering the trajectories of different isotopic chains in the IBA symmetry triangle and the lines corresponding to the X(3), X(5)-β^2, and X(5)-β^4 models, seen in Fig. 1, and in addition, the best agreement for $R_{0/2} = E(0_2^+)/E(2_1^+)$. We identify ^{186}Pt and ^{172}Os as candidates for the X(3) model, ^{146}Ce and ^{174}Os as candidates for the X(5)-β^2 model, and ^{158}Er and ^{176}Os as candidates for the X(5)-β^4 model. The experimental level schemes of these nuclei are compared to the relevant geometrical model predictions as well as IBA calculations in Figs. 3-5.

Considering that these nuclei were essentially chosen on the basis of only their $R_{4/2}$ ratio and $R_{0/2}$ ratio, the level of agreement for the other experimental observables is quite impressive. Overall the spacings in the K = 0_2^+ excited sequence are well reproduced by both the geometrical models and the IBA calculations. The one exception is in ^{172}Os, where experimentally the first two levels of the K = 0_2^+ band are lying too close, resulting in $R_{4/2} \sim 7$, which cannot be correct, indicating that the experimental information on these levels should be reconsidered. The X(3) model shows excellent agreement with the yrast band $B(E2)$ values in ^{186}Pt and ^{172}Os, whereas the IBA significantly underpredicts them. Identical results are found for the yrast band $B(E2)$ strengths in ^{158}Er (compared with the X(5)-β^4) model). In ^{174}Os, the yrast $B(E2)$ strengths are overestimated by the X(5)-β^2 model, while the IBA calculations provide a reasonable description. The branching ratios from excited states in the K = 0_2^+ sequence are also well reproduced by the geometrical models. Overall, each of these candidate nuclei present an enhanced decay to the spin-ascending branch and a suppression to the spin-descending branch, in agreement with the predictions of X(3), X(5)-β^2, and X(5)-β^4. The IBA calculations also generally follow this pattern, with the exception of the predictions for ^{174,176}Os.

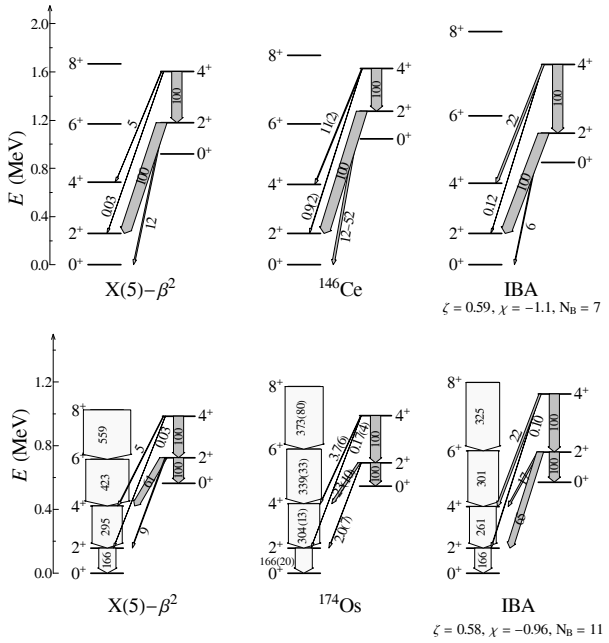

Figure 4. Same as Fig. 3, but for comparison of the experimental data (middle) to the X(5)-β^2 predictions (left) and IBA calculations (right) for ^{146}Ce (top) and ^{174}Os (bottom). Experimental data taken from Refs. [35,36].

Given the narrowness of the shape/phase transition region of the IBA, it is not surprising that good experimental examples of X(3), X(5)-β^2, and X(5)-β^4 are provided by neighboring even-even nuclei (^{172}Os–^{174}Os–^{176}Os). The IBA total energy curves for these nuclei, obtained from Eq. (3) and the parameters given in the captions of Figs. 3-5, are shown in Fig. 6. With increasing neutron number, the total energy curves evolve from a shallow deformed minimum in ^{172}Os to more pronounced single deformed minima in ^{174,176}Os. Qualitatively speaking, the evolution of these potentials resembles the evolution of the potentials one would obtain in moving from X(3) to X(5)-β^2, to X(5)-β^4, namely a flat bottomed potential in X(3) followed by a potential where the single deformed minimum becomes larger, as in X(5)-β^2 and X(5)-β^4. More specifically, the slight preference for a deformed minimum in ^{172}Os suggests that it lies actually just beyond $\zeta = \zeta_{\rm crit}$ within the IBA space. In fact, the parameters obtained in the fit to ^{172}Os are consistent with the parameters obtained for the "best fit" of the X(3) solution corresponding to ζ^{**}.

5. DISCUSSION

In the present work the parameter independent (up to overal scale factors) predictions of the X(5)-β^2, X(5)-β^4, and X(3) models are compared to the results of two-parameter

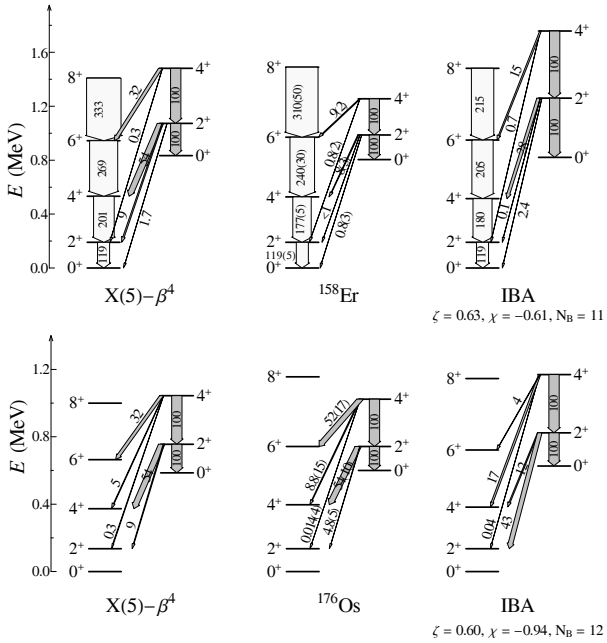

Figure 5. Same as Fig. 3, but for comparison of the experimental data (middle) to the X(5)-β^4 predictions (left) and IBA calculations (right) for ^{158}Er (top) and ^{176}Os (bottom). Experimental data taken from Refs. [37,38].

interacting boson approximation (IBA) model calculations, with the aim of establishing a connection between these two approaches. The study is focused on boson numbers of physical interest (around 10). It turns out that both X(3) and X(5)-β^2 lie close to the U(5)–SU(3) leg of the IBA symmetry triangle and within the narrow shape/phase transition region of the IBA. In particular, for $\chi = -1.32$, X(3) lies close to $\zeta_{\rm crit}$, the left border of the shaded shape/phase transition region of the IBA, corresponding to IBA total energy curves with two equal minima, while X(5)-β^2 lies near the right border of the shape/phase transition region, ζ^{**}, corresponding to IBA total energy curves with a single deformed minimum. A set of neighboring even-even nuclei exhibiting the X(3), X(5)-β^2, and X(5)-β^4 behaviors have been identified (^{172}Os-^{174}Os-^{176}Os). Additional examples for X(3), X(5)-β^2, and X(5)-β^4 are found in ^{186}Pt, ^{146}Ce, and ^{158}Er, respectively. The level of agreement of these parameter free, geometrical models with these candidate nuclei is found to be similar to the predictions of the two-parameter IBA calculations.

It is intriguing that the X(3) model, which corresponds to an *exactly separable* γ-rigid (with $\gamma = 0$) solution of the Bohr collective Hamiltonian, is found to be related to the IBA results at $\zeta_{\rm crit}$, which corresponds to the critical case of two degenerate minima in the IBA total energy curve, approximated by an infinite square well potential in the model. It is also remarkable that the X(5)-β^2 model, which uses *the same approximate separation of*

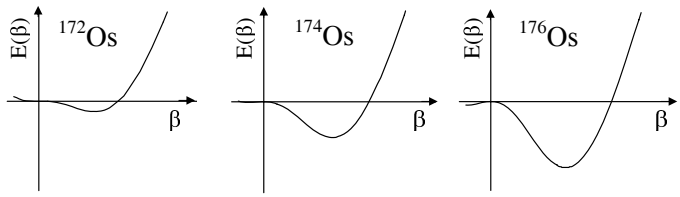

Figure 6. IBA total energy curves for ^{172}Os (left), ^{174}Os (middle), and ^{176}Os (right) obtained from Eq. (3) using the parameter sets quoted in the captions of Figs. 3-5.

variables as the X(5) critical point symmetry, is found to correspond to the right border (ζ^{**}) of the shape/phase transition region, related to the onset of total energy curves with a single deformed minimum, comparable in shape with the β^2 potential used in the model in the presence of a $L(L+1)/(3\beta^2)$ centrifugal term [8].

Comparisons in the same spirit of the parameter independent predictions of the E(5) critical point symmetry [1] and related E(5)-β^{2n} models [39,40], as well as of the related to triaxial shapes Z(5) [41] and Z(4) [42] models, to IBA calculations and possible placement of these models on the IBA-1 symmetry triangle (or the IBA-2 phase diagram polyerdon [43–45]) can be illuminating and should be pursued.

It should be noticed that the present work has been focused on boson numbers equal or close to 10, to which many nuclei correspond. A different but interesting question is to examine if there is any connection between the X(3), X(5)-β^2, and/or X(5)-β^4 models and the IBA for large boson numbers. This is particularly interesting especially since it has been established (initially for $N = 1,000$ [39], recently corroborated for $N = 10,000$ [46]) that the IBA critical point of the U(5)-O(6) transition for large N corresponds to the E(5)-β^4 model, i.e. to the E(5) model employing a β^4 potential in the place of the infinite well potential.

REFERENCES

1. F. Iachello, Phys. Rev. Lett. 85 3580 (2000) 3580.
2. F. Iachello, Phys. Rev. Lett. 87 (2001) 052502.
3. R. F. Casten and N. V. Zamfir, Phys. Rev. Lett. 85 (2000) 3584.
4. R. M. Clark et al., Phys. Rev. C 69 (2004) 064322.
5. R. F. Casten and N. V. Zamfir, Phys. Rev. Lett. 87 (2001) 052503.
6. R. M. Clark et al., Phys. Rev. C 68 (2003) 037301.
7. M.A. Caprio, Phys. Rev. C 69 (2004) 044307.
8. M.A. Caprio, Phys. Rev. C 72 (2005) 054323.
9. N. Pietralla and O.M. Gorbachenko, Phys. Rev. C 70 (2004) 011304(R).
10. D. Bonatsos, D. Lenis, N. Minkov, P. P. Raychev, and P. A. Terziev, Phys. Rev. C 69 (2004) 014302.
11. D. Bonatsos, D. Lenis, D. Petrellis, P. A. Terziev, and I. Yigitoglu, Phys. Lett. B 632 (2006) 238.

12. D. H. Feng, R. Gilmore, and S. R. Deans, Phys. Rev. C 23 (1981) 1254.
13. F. Iachello and A. Arima, The Interacting Boson Model, Cambridge University Press, Cambridge, 1987.
14. J. N. Ginocchio and M. W. Kirson, Phys. Rev. Lett. 44 (1980) 1744.
15. A. E. L. Dieperink, O. Scholten, and F. Iachello, Phys. Rev. Lett. 44 (1980) 1747.
16. R. F. Casten, Nuclear Structure from a Simple Perspective, Oxford University Press, Oxford, 1990.
17. F. Iachello, N. V. Zamfir, and R. F. Casten, Phys. Rev. Lett. 81 (1998) 1191.
18. N. V. Zamfir, P. von Brentano, R. F. Casten, and J. Jolie, Phys. Rev. C 66 (2002) 021304.
19. F. Iachello and N. V. Zamfir, Phys. Rev. Lett. 92 (2004) 212501.
20. V. Werner, P. von Brentano, R. F. Casten, and J. Jolie, Phys. Lett. B 527 (2002) 55.
21. N. V. Zamfir and G. E. Fernandes, in Proceedings of the Eleventh International Symposium on Capture Gamma Ray Spectroscopy and Related Topics (Prohonice, 2002), edited by J. Kvasil, P. Cejnar, and M. Krticka, World Scientific, Singapore, 2003.
22. J. Y. Zhang, R. F. Casten, and N. V. Zamfir, Phys. Lett. B 407 (1997) 201.
23. E. A. McCutchan, N. V. Zamfir, and R. F. Casten, Phys. Rev. C 71 (2005) 034309.
24. E. A. McCutchan, N. V. Zamfir, and R. F. Casten, Phys. Rev. C 69 (2004) 064306.
25. A. Bohr, Mat. Fys. Medd. K. Dan. Vidensk. Selsk. 26 (1952) no. 14.
26. E. López-Moreno and O. Castaños, Phys. Rev. C 54 (1996) 2374.
27. D. J. Rowe, Nucl. Phys. A 735 (2004) 372.
28. D. J. Rowe, P. S. Turner, and J. Repka, J. Math. Phys. 45 (2004) 2761.
29. D. J. Rowe and P. S. Turner, Nucl. Phys. A 753 (2005) 94.
30. E. A. McCutchan and N. V. Zamfir, Phys. Rev. C 71 (2005) 054306.
31. E. A. McCutchan, R. F. Casten, and N. V. Zamfir, Phys. Rev. C 71 (2005) 061301(R).
32. C. M. Baglin, Nucl. Data Sheets 99 (2003) 1.
33. J. C. Walpe, PhD. Thesis, University of Notre Dame, 1999.
34. B. Singh, Nucl. Data Sheets 75 (1995) 199.
35. L. K. Peker and J. K. Tuli, Nucl. Data Sheets 82 (1997) 187.
36. E. Browne and Huo Junde, Nucl. Data Sheets 87 (1999) 15.
37. R. G. Helmer, Nucl. Data Sheets 101 (2004) 325.
38. M.A. Basunia, Nucl. Data Sheets 107 (2006) 791.
39. J. M. Arias, C. E. Alonso, A. Vitturi, J. E. García-Ramos, J. Dukelsky, and A. Frank, Phys. Rev. C 68 (2003) 041302.
40. D. Bonatsos, D. Lenis, N. Minkov, P. P. Raychev, and P. A. Terziev, Phys. Rev. C 69 (2004) 044316.
41. D. Bonatsos, D. Lenis, D. Petrellis, and P. A. Terziev, Phys. Lett. B 588 (2004) 172.
42. D. Bonatsos, D. Lenis, D. Petrellis, P. A. Terziev, and I. Yigitoglu, Phys. Lett. B 621 (2005) 102.
43. J. M. Arias, J. E. García-Ramos, and J. Dukelsky, Phys. Rev. Lett. 93 (2004) 212501.
44. M. A. Caprio and F. Iachello, Phys. Rev. Lett. 93 (2004) 242502.
45. M. A. Caprio and F. Iachello, Ann. Phys. (NY) 318 (2005) 454.
46. J. E. García-Ramos, J. Dukelsky, and J. M. Arias, Phys. Rev. C 72 (2005) 037301.